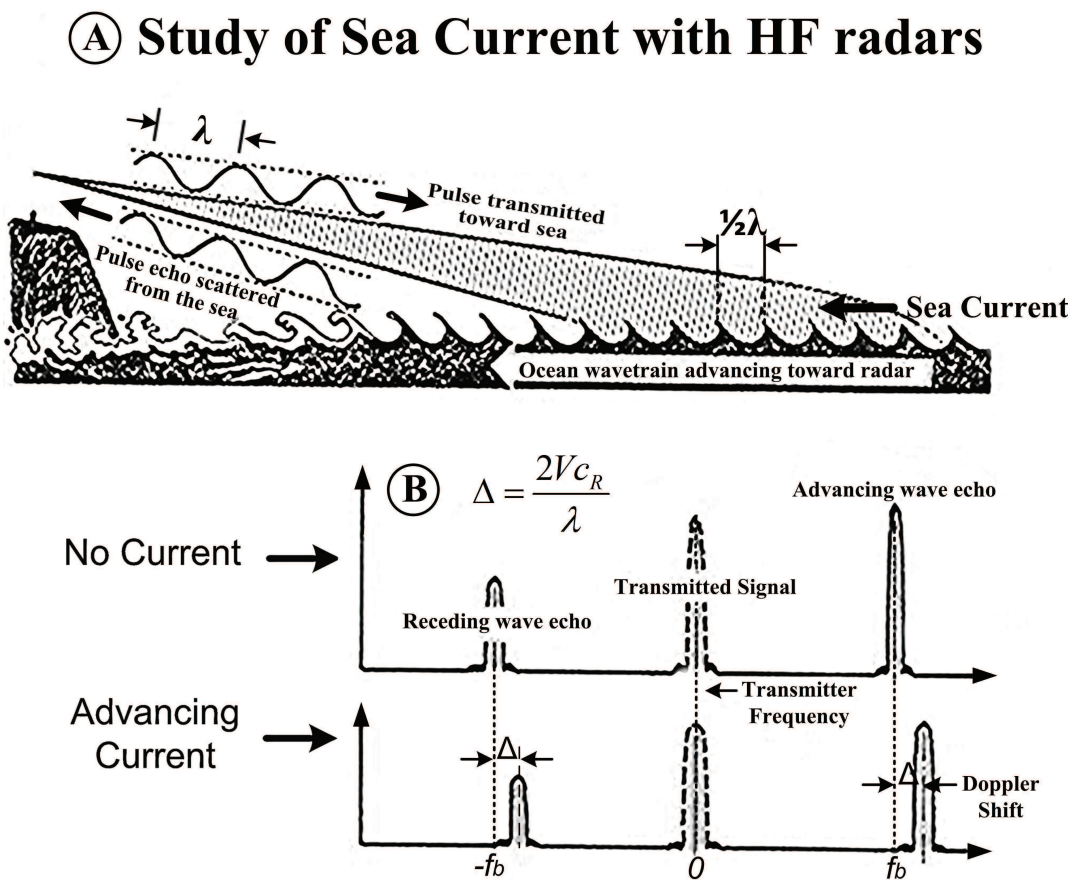

Figure 3.18. *Study of sea surface currents with an HF radar system.* **(A)** sketch of the principle of an HF OTHR-GW system. **(B)** First order component of the Sea Spectrum in two different cases: no radial component of surface current (top) and presence of a surface current in the direction moving toward the radar (bottom).

– *propagation speed*[7]: distance covered by a crest in the time unit;

– *period*: time interval between the passage from the same point of two consecutive crests.

Figure 3.18 shows a sketch of the geometry of an HF coastal system and its usage for "Sea Observation" purposes. In the lower part of the picture it is proposed the mechanism employed by the radar to estimate the *propagation speed*. The two spectral components that in absence of radial component of the sea surface current have frequency $\pm f_b$ are referred to as *"Bragg Components"* or *"Bragg*

[7]Note that in case of the employment of a single HF sensors it would be more appropriate to consider only the *radial component* of the propagation speed.

Lines". Their deviation Δ from the expected value is proportional to the actual radial component of the sea-waves propagation speed.

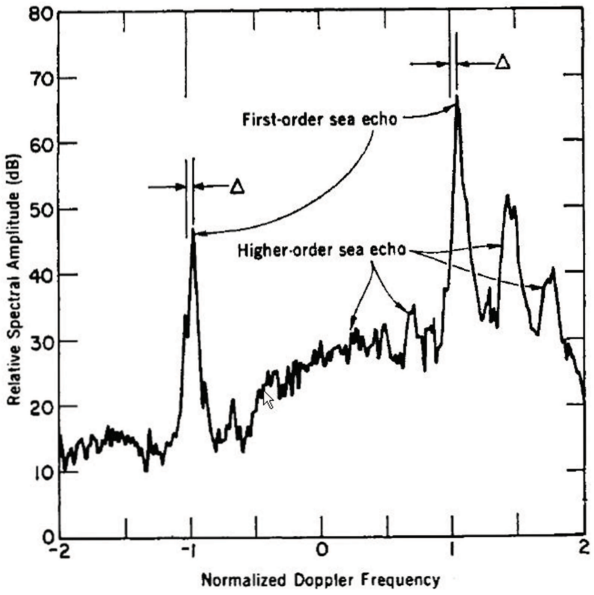

Figure 3.19. *Normalized Doppler Spectrum of Sea Surface Backscattering at a frequency of 9.4 MHz*: The carrier is centred in 0 Hz, while ± 1 corresponds to a Doppler shift of ± 0.313 Hz. The frequency resolution is 0.01 Hz. [30, 46, 52, 18, 48].

Fig. 3.19 shows an example of Sea Spectrum in the HF band. From the picture we can make some consideration:

- The dominant *First-Order* peaks (located close to ± 1) are related to gravitational oceanic waves with lenght $L \approx 16$ m:
  $L = \frac{\lambda}{2} = \frac{c}{2f} = \frac{2.99 \cdot 10^8}{2 \cdot 9.4 \cdot 10^6} = 15.9$ m;
- the peaks location in proximity of ± 1 suggests a Doppler shift $f_b = \pm 0.313$ Hz, that corresponds to a radial component of the sea-wave speed s: $s_r = \frac{f_b \cdot \lambda}{2} = \frac{0.313 \cdot 31,8}{2} \approx 5$ m/s;
- the actual distance of the two peaks from ± 1, denoted with Δ, is proportional to the radial component of the Sea Current: $\Delta = \frac{s_r}{\lambda}$;
- some characteristics of the Higher-Order spectral components (i.e. shape, peaks position, peaks amplitude, etc.) can be employed to estimate the *Sea State*.

The intensity of the sea clutter in a given maritime region is strongly related to the Sea State value in that same region. The Sea surface shows a double gradient of the backscattering coefficient σ_m:

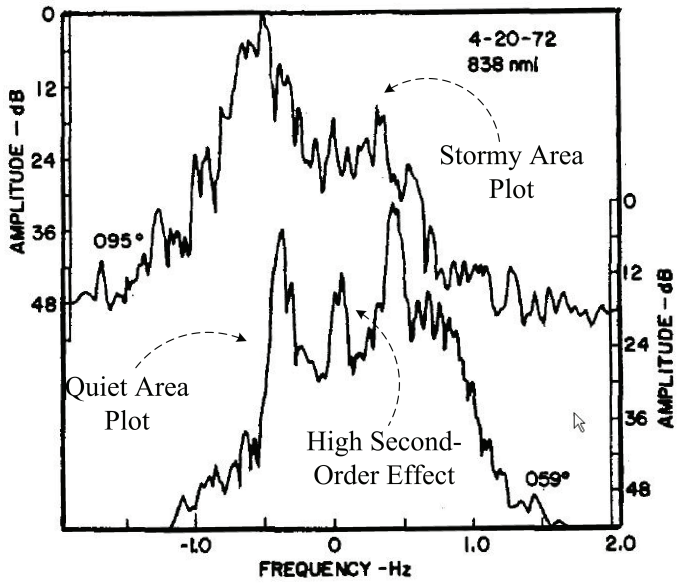

Figure 3.20. *Normalized Doppler Spectrum of Sea Surface Backscattering for two different azimuthal directions*: The upper curve is relative to a "stormy" sea region, while the lower curve is relative to a region with a reduced sea activity. [30]

– a spatial gradient. Fig. 3.20 shows two different Sea Spectrum relative to different azimuthal pointing directions.

– a temporal gradient. This latter is generally characterized by really low values, since the Sea State in a given area changes really slowly.

Land Clutter

For what concerns the land clutter in the HF band it was remarkably difficult for us to gather any information, especially when related to "high" (greather than ten degrees) angles of incidence.
It was possible to find in literature some paper on the performance of land clutter suppression-methods, but in general, the documentation refers to millimetric waves and considers two different scenarios: ground radar with low angles of incidence [68]; ship-borne radar for the study of coastal profiles [41].

The magnitude of the specific backscattering coefficient relative to a land area depends on the superficial characteristics of the soil and on the slope of the ground in the considered area.
According to the geometric optics laws, the intensity of the backscattered signal is proportional to the angle between the incident direction and the reflection sur-

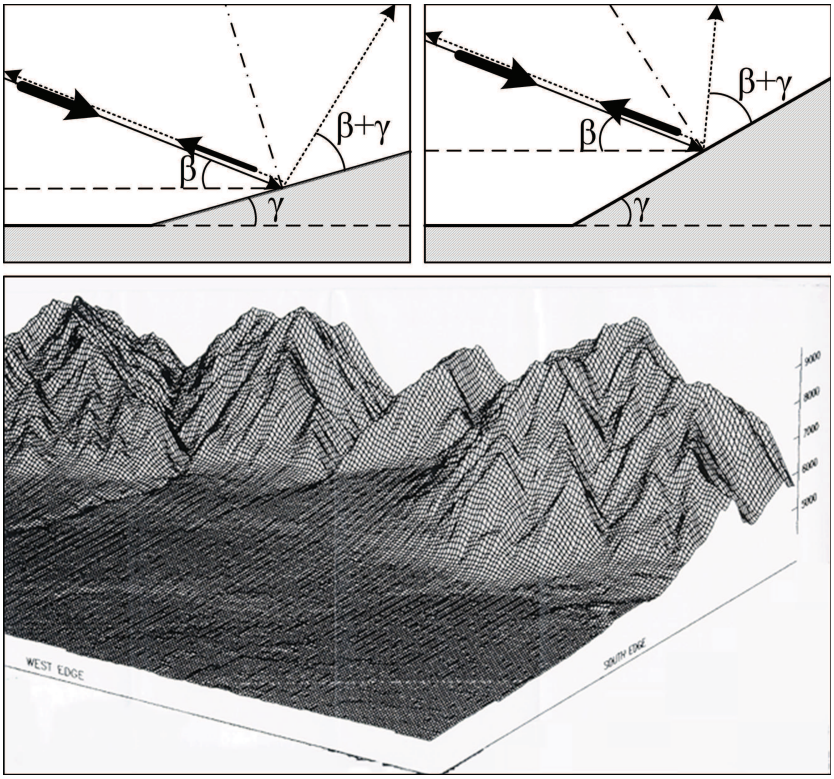

Figure 3.21. Top: Scattering mechanism and its dependency upon the ground slope and the signal incidence angle. Bottom: an example of Digital terrain Elevation Model (DEM).

face. This angle is given by the sum between the take-off angle (that, according to the chosen geometry, is identical to the incidence angle) and the slope of the ground at the point of incidence of the signal. For example, if we refer to the simplified sketch proposed in the top part of fig. 3.21, it appears evident that, assuming the same type of soil, for the geometry represented in the right side of the picture, where the land's slope is greater, we have a higher intensity of the backscattered component.

In this case we considered two land region whose surface is free from any eventual element, but in general, in order to properly estimate the backscattering properties of a given land region, it is really important also to consider all those elements with overall dimensions comparable to a half of the signal wavelength. Since in the HF band trees, pylons, buildings with multiple floors, etc. .. generally meet these conditions, a desert area will be in general characterized by a backscattering coefficient different from that of a forest area or from that of an urban center with the same surface.

Considerations on the Clutter Model

The present research is based upon the ability of an OTHR-SW system to identify and locate in the received echo the eventual presence of sea/land transitions. The method takes advantage from the discontinuity in the backscatter coefficient between land and sea areas and then from the consequent irregularity within the clutter profile that characterizes a sea/land region.
A brake to the development of the method is the lack of information about the actual magnitude and distribution of the backscatter coefficient in the HF band. In this regard it is therefore desirable a study, similar to that presented in [20] (unfortunately relative to frequencies higher than those of interest), suitable to identify the average values of the backscatter coefficient for different types of ground and with different terrain-slopes (aka "depression angles").
The entire work presented here is based upon simulated data, hence also the distribution of the backscattering coefficient in the selected area follows some model hypothesis. Fig. 3.22 shows two possible methods for simulating the spatial distribution of the backscattering coefficients in a rectangular region that considers both sea and land areas. The first method is the one employed in the simulations presented in the following chapters and it is based upon a binary classification of the clutter. The second method represents an evolution of the previous one and considers a characterization of the area of interest with multiple backscattering coefficients for sea and land areas.

Assuming a binary distribution of σ, then the normalized backscattering coefficient for a *resolution patch* ΔS characterized by both sea and land is evaluated following the example provided by fig. 7.6.

Generally the clutter power is expressed as [49]:

$$Pc = K \cdot \frac{\sigma_0 F^4 Ac}{R^4}$$

where:

- K is a constant factor defined by the transmitted power, the antenna's gain, the signal's wavelength and the system's losses;
- F^4 represents the two-ways propagation factor;
- R is the one-way slant-range distance between the radar-site and the radar-footprint;
- Ac is the surface of the radar resolution cell referred to as "Clutter Area" (we assume that this region is limited in range by the pulse projection to the ground, according to figure 7.4);

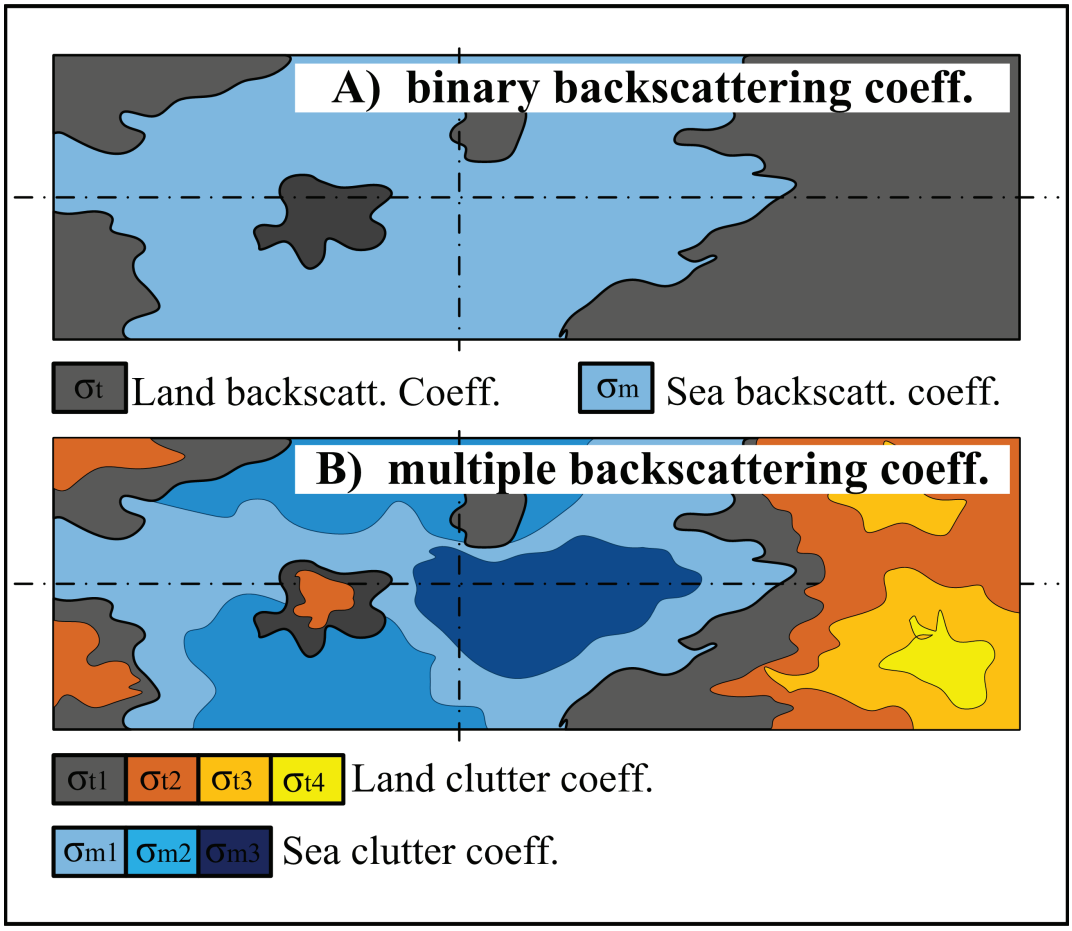

Figure 3.22. *Differences in the employment of a binary or multivalued mask of the HF backscattering coefficient.*

– σ_0 represents here the specific backscattering coefficient, expressed as the averaged value of the backscattering coefficients relative to the n sectors of surface ΔS in which the region Ac has been divided:

$$\sigma_0 = \frac{1}{n} \cdot \sum_{i=1}^{n} \sigma_{0i}$$

Considering σ_0 as the superposition of multiple contributes is particularly useful in OTHR-SW applications, where the radar footprint and the *Clutter Area* assume large dimensions, including regions characterized by different values of the backscattering coefficient. From the last equations appears evident as the availability of a backscattering coefficients database relative to the OTHR-SW surveillance area, and realized for multiple values of frequency and incidence angle, can be employed to evaluate the clutter power contribution relative to any

given surface element.

Several papers propose a different classification of the surface clutter based upon its spectral occupation. A binary classification considers two clutter contributions of different nature, indicated as: *"clustered clutter"* and *"distributed clutter"*.

The clutter discrimination between sea and land toward the *Range-Doppler* analysis of the radar echo seems to be a well consolidated technique. In fact, as we previously described, while the Doppler spectrum of the land shows an extremely narrow band (centred in $f_d = 0$ Hz), the sea Doppler spectrum typically shows a larger band centred in correspondence to the Bragg's line (see figures 3.19 and 3.20).
This fact is certainly precious during the Doppler analysis of the received echo and it allows a quite simple discrimination, but unfortunately it cannot be exploited by the presented research, since it requires a processing time that is not allowed in real-time applications as the proposed SLTI method.

3.3.7 Targets of Interest

In this section are presented several typical targets of interest for an OTHR-SW system. For all these targets a general overview of the principal physical and cinematic features is given.

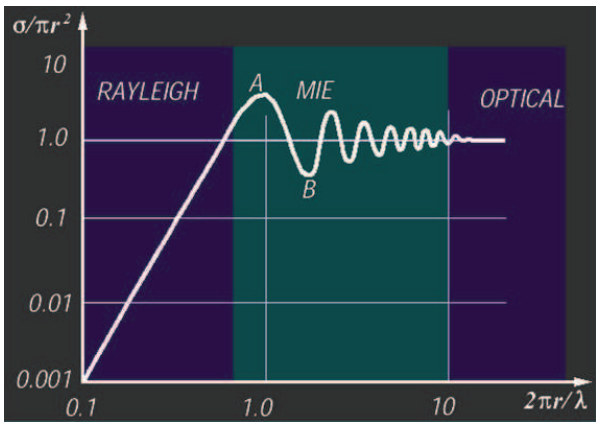

Figure 3.23. *Normalized Backscattering Profile* of a metallic sphere of radius r.

As for each different radar sensor, the image of a given target is referred to as "Radar Cross section" (RCS) and it is strongly dependent upon the radar operative frequency. Hence the same target can appear in two different ways to the same radar if it employs two different values of frequency. Figure 3.23 shows

the normalized backscattering profile (that is the normalized RCS σ) for a really simple shaped target: a metallic sphere of radius r. On a double logarithmic scale the various *"frequency regions"* of the sphere are introduced:

- in the *"Optical Region"* the RCS appears to be constant ($\sigma = \pi r^2$), independently from the frequency (hence from the relative wavelength λ);
- in the "A" point, pertinent to the *"Mie Region"* (aka "Resonance region"), there is the σ maximum that corresponds to four times the value assumed in the *"Optical Region"*;
- in the *"Rayleigh Region"* the RCS value grows in a regular way until it reaches its maximum at the boundary with the Mie Region.

There are different types of targets of interest for an OTHR-SW sensor and their characteristic parameters can vary in a large range of values: just think about an air superiority fighter and a cargo ship and their respective size and cruise speed. In table 3.1 are shown, simply by way of illustration, the main geometric and cinematic characteristic parameters for some possible targets of interest. The very large range of values of these quantities appears evident.

Target	**Type and Use**	**Speed [km/h]**	**Length [m]**	**Width [m]**	**Height [m]**
B-52H *Stratofortress*	Strategic Bomber	820	49	56	12
Boeing 737-900ER	Intercont. Transport Passengers	960	42	35	12.5
F-22 *Raptor*	Air Superiority Fighter	1960	19	13.5	5
F-117 A *NightHawk*	Stealth Bomber	1000	20	13	4
Piper Seminole	Helix Twin-Engine	300	8.5	12	2.5
Nimitz Class A.C.	Nuclear Aircraft Carriers	56	340	78	40

Table 3.1. Example of targets of interest for an OTHR-SW system, together with some of their geometric and cinematic parameters.

To work with a wide set of targets it's necessary to be able to change with extreme agility the main radar parameters (bandwidth, frequency, transmission power, coherent observation period, etc.).

Historically OTHR-SW systems were born as a early-warning sensors [32] and they were therefore optimized for very fast targets (which can strike from a distance and short term): long-range bombers, intercontinental ballistic missiles, etc.
Later, many advances in the *signal processing* techniques and the improvement in *target tracking procedures* allow OTHR-SW to monitor air and sea traffic in its vast coverage area.

As previously mentioned, the extreme variability of RCS and Doppler signature of the considered targets requires a strong adaptation capability of the radar system. During the operational phase it can be necessary to vary the size of the beam or the intensity of the transmitted power, or even the duration of the pulse and its repetition frequency.
The ability to detect any targets in downlink (i.e. from top to bottom) allows the OTHR-SW to reveal targets that are "invisible" to other radars, like civilian aircraft of small size, capable of flying at low altitude between the reliefs, making them ideal for drug traffic activities [24].

Note that working in the HF band [8] means that the target's RCS depends on its overall dimensions and not on the type of material (roughness) and conformation of its surface. This makes the current *"stealth"* techniques (adopted for instance on aircrafts as F-117A, F-22, etc., but also on maritime high speed vessels) ineffective for OTHR-SW applications.

In fig. 3.24 some examples of stealth targets are shown. In clockwise order from top-left:

- two *F-22 Raptors* produced by Lockheed Martin - Boing;
- a *F-117A "Nigthawk" Fighter* in force to USAF;
- a *Houbei Class Missile Boat* in force to Chinese Navy;
- two *Visby Class Corvettes* in force to the Royal Swedish Navy.

Algorithms for calculating the RCS of a target in the HF band generally carry out a breakdown of the considered target into basic geometric solids [9] [22] and then they employ the principle of effects superposition to evaluate the entity of the parameter.

Unfortunately creating a database of RCS for the targets of interest of OTHR-SW systems seems to be a really complicated task. In fact this parameter depends not only from the working frequency [10] (see Fig. 3.23), but also from the angle

[8] The HF band [3,30] MHz correspond to wavelengths ranging from ten to hundred meters

[9] An airliner can, for example, be represented by the set of a cylinder (fuselage), and three cubes (wings and rudder).

[10] In the HF band the RCS can vary by 2-3 orders of magnitude depending on its position inside or outside the *Resonance region*.

Figure 3.24. An example of "stealth" targets. The stealth technique is developed against μ−wave radars and it is ineffective against HF radar systems.

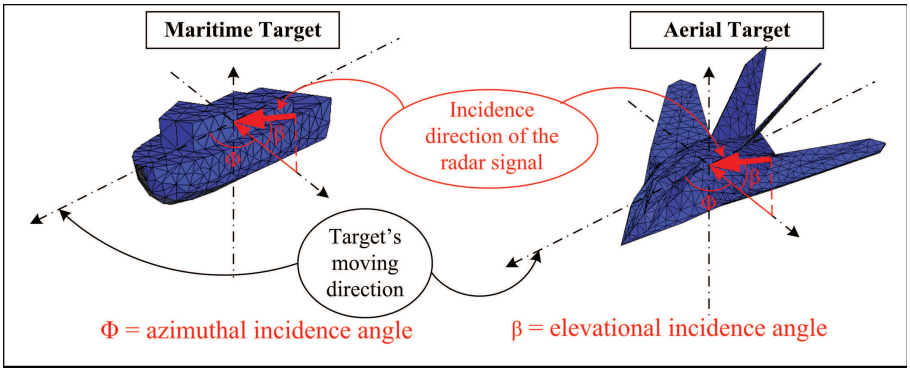

Figure 3.25. Sketch of the geometry of target's illumination by the radar.

at which the target is illuminated by the radar (fig. 3.25). For example, the RCS of the *left through* of a boat will be similar to that of its *right through*, but totally different from that of the same boat viewed *bow*-side (or *stern*-side).
Here we are not discussing in detail the arguments *"Targets"* and *"RCS"* since they are separated from the georeferencing technique that we want to introduce.